Microbial mat contribution to the formation of an evaporitic environment in a temperate-latitude ecosystem

Vanesa Liliana Perillo[1,2,*], Lucía Maisano[1,3], Ana María Martinez[4,5], Isabel Emma Quijada[6], Diana Graciela Cuadrado[1,3]

[1]Instituto Argentino de Oceanografía (IADO-CONICET-UNS), Camino La Carrindanga km 7 E1, Bahía Blanca, Argentina, B8000CPB;

[2]Departamento de Biología, Bioquímica y Farmacia, Universidad Nacional del Sur, San Juan 670 Piso 1, Bahía Blanca, Argentina, B8000ICN;

[3]Departamento de Geología, Universidad Nacional del Sur, Alem 1253 Piso 2, Cuerpo B, Bahía Blanca, Argentina, B8000ICN;

[4]Departamento de Química, Universidad Nacional del Sur, Av. Alem 1253 Planta Baja, Bahía Blanca, Argentina, B8000CPB;

[5]Instituto de Química del Sur (INQUISUR-CONICET-UNS), Av. Alem 1253, Bahia Blanca Blanca, Argentina, B8000CPB;

[6]Deptartamento de Geología, Universidad de Oviedo, C/ Jesús Arias de Velasco s/n, 33005 Oviedo, España.

[*]Corresponding author: vperillo@criba.edu.ar

Abstract

An evaporitic environment is characterized by having high salinity, climatic, and hydrological factors that promote a negative water balance; however, biological factors may also influence their development. Modern coastal flat Paso Seco (40°33′S; 62°14′W) is located in a semi-arid region with low precipitation and dry winds coming mainly from the NW. The site is an old tidal channel, which nowadays behaves like a shallow coastal saline-like basin, separated from the sea by a sand barrier, which the sea periodically overcomes, flooding the flat with eventual water evaporation. Microbial mats of up to 1 cm thick colonize the sandy sediments of this evaporitic environment. Water samples were taken during five field trips (2017-2018) from interstitial water of the flat, a tidal creek that crosses the flat, and two shallow tidal depressions (TDs) within the flat with different degrees of evaporation. In comparison to the sea, the maximum salinity values measured in Austral spring (September 2017) in the tidal creek were doubled, tripled in interstitial water, and 5.9 to 8 times higher in TDs. Ionic concentration denotes that evaporite chemical divides are followed as water evaporates, corresponding to the presence of $CaCO_3$, gypsum and halite found in TDs. On-site permeability of microbial mat-covered surfaces presented semi-pervious properties. Microbial mat presence is condition for $CaCO_3$, gypsum, and halite precipitation as they allow for water retention and its consequent evaporation due to the impermeability they confer to the sedimentary surface. Thus, microbial mats are a biological factor affecting the development of an evaporitic environment.

Keywords: Saline basin; Evaporite; Calcium carbonate; Water retention; Salinity

1. Introduction

Evaporites in a broad sense are a "group of sedimentary deposits whose origin is largely due to evaporation" (Twenhofel, 1950). In the case of marine evaporites, seawater molecules evaporate following the Usiglio sequence for salt precipitation, resulting first in aragonite and calcite precipitation, then in gypsum and later halite precipitation (Dean, 2013; Usiglio, 1849). Present-day marginal marine evaporite deposits are mainly located within two subtropical high-pressure belts (between 15˚ and 35˚ latitude from the equator), where there is limited rainfall and elevated evaporation (Babel and Schreiber, 2014). Examples of these environments are the sabkhas of the Red Sea coastal tidal flats of Saudi Arabia and Abu Dhabi, and coastal saline basins in Southern Australia, among others (Aref and Taj, 2017; Butler et al., 1987; Orti, 2010; Shearman, 1978; Strohmenger et al., 2010; Warren, 2016a, 2016b).

Marginal marine evaporites are being deposited nowadays in coastal salinas (sub-sea level depressions separated from the sea by a barrier and supplied by seawater, in which subaqueous evaporites are formed; Warren, 2016a) and coastal sabkhas (supratidal flats in which intra-sedimentary evaporites are formed; Warren, 2016). A negative water balance is a condition for the formation of these evaporite environments, where outflow of water should be higher than the inflow of any kind of water – marine or otherwise (Babel and Schreiber, 2014).

Temperature, salinity, and pH are the main physicochemical parameters that characterize evaporite environments, and these parameters must vary in a way that they promote supersaturation and precipitation of the ions in solution (Babel and Schreiber, 2014). Low relative humidity, for example, is needed for halite precipitation, while in a restricted evaporite setting, the presence of gypsum suggests evaporation at temperatures lower than 30 ˚C (Kinsman, 1976; Krumbein and Garrels, 1952). However, beyond climatic and purely physical

hydrological features, biological factors could also influence the hydrology of a site, indirectly contributing to the conditions needed for the formation of evaporite environments.

Microbial mats are photosynthetic associations of prokaryotes, archaea and eukaryotes, dominated mainly by cyanobacterial species, which commonly colonize supratidal sediments, flooded intermittently. Cyanobacteria are the primary producers of extracellular polymeric substances (EPS) that help trap, bind and precipitate sediments and minerals (Stolz, 2000). This physicochemical matrix is composed of secreted polysaccharides, proteins, lipids, DNA, and vitamins (Flemming and Wingender, 2001), offering several uses for bacteria, such as chelation of toxic ions and sheltering from harmful UV radiation (Decho, 2011; Or et al., 2007). EPS has indirectly been shown to protect from desiccation for its high water retention capacity, as mutations in EPS biosynthesis genes decrease desiccation tolerance and such water conditions result in increased EPS production (Schnider-Keel et al., 2001; Alvarez et al., 2004; Or et al., 2007; Decho, 2011). The combination of bacteria, EPS and trapped sediments that form microbial mats creates a poorly permeable sediment surface (Bąbel, 2007), slowing water percolating from the surface over periods of time. That fact is reflected in the flat of Paso Seco by the formation of special microbially sedimentary structures, such as gas domes (Noffke, 1999), which prevent the escape of gases (Cuadrado et al., 2013).

However, although in many evaporitic environments around the world microbial mats are being studied (e.g., in sabkhas; Aref and Taj, 2017, 2018), their presence is only considered in the light that they are present as a consequence of the hydrodynamics of the site, and how they chemically affect the environment (Babel, 2004; Long et al., 2009), but do not incorporate into their studies the possible effect they have in modifying the hydrodynamics of the site as well.

In evaporite environments, water retention is vital for precipitation of evaporite minerals. Without water retention, the dissolved ions needed for evaporite formation would percolate into the sediment with water. Thus, in this work, we propose that the presence of microbial mats in the temperate coastal flat Paso Seco (Argentina) is essential for the formation of the evaporite deposits found in the site. Although the local climatic factors are enough for evaporite formation, especially the constant and powerful drying winds, without microbial mats there would not be enough water retention to allow for the concentration of ions and their precipitation through evaporation. These results document the biogeochemical control in hydrology in a geomorphological restricted basin and how biological factors could potentially change the hydrological conditions of an evaporitic environment.

2. Material and methods

2.1. Study site and water sampling period

Water sampling was performed to characterize the environment on May, September and October 2017, and March and June 2018 at two stations, 3 and 4, and from a tidal creek located close to St. 3 (‘St. 3’ and ‘St. 4’, and ‘St. 3 Tidal Creek’, respectively from now on; Fig. 1), in a temperate coastal flat at Paso Seco, Argentina (40°33′S; 62°14′W; Fig 1), located in northern Patagonia. The climatic region where Paso Seco is situated is considered as semiarid, according to the recent climatic classification of the Argentinian Pampas proposed by Aliaga et al. (2017). The average maximum high temperature is 30 °C in summer and 12 °C in winter, while average low temperatures are 14 and 2 °C, respectively (‘Servicio Meteorologico Nacional, ’ n.d.). The average annual rainfall is 300 mm but is characterized by large space-time variation, raining for a total of 80 days throughout the year in average (Ferrelli et al., 2012, ‘Servicio Meteorologico Nacional, ’ n.d.). Potential evapotranspiration in the region exceeds precipitation, with aridity

strong enough to limit vegetation development. The SW Atlantic Ocean moderates the differences between summer and winter, preventing extreme hot and cold conditions. Strong NW winds prevail in the area, averaging a maximum of 44 km h^{-1} with frequent gusts up to 100 km h^{-1} in the last five years (unpublished data). Geomorphologically, the study area comprises a sizeable closed basin (about 2.5 × 0.3 km), colonized by microbial mats and choked by a 1.8 km-wide sand spit formed by NE longshore sediment transport. Whenever strong winds combine with the effect of the spring tides or storms, seawater is pushed through the sand spit to enter the water into the basin, resulting in the flooding of the study area (Cuadrado et al., 2015). Sediment of the flat is predominantly sandy, and most of the surface of the flat is covered by microbial mats. The force of the flooding usually results in a large number of elongated tidal depressions (TDs, Fig. 2a), as classified by Perillo (2018), re-colonized by microbial mats. Other microbial sedimentary structures such as erosional pockets (Noffke, 1999) where the sediments have little colonization and can be found covered by ripples (Fig. 2b). The study site was found flooded both in May 2017 and June 2018 during field trips. Weather data (air temperature and wind speed) were taken from the Global Forecast System model provided by the website Windguru at the closest weather station to the site, located at El Condor, Río Negro, Argentina (40° 55' 43.32" S, 64° 23' 31.92" W).

2.2. Water level and permeability

Water-level fluctuations in the groundwater and also by tidal inundation of the study area have been measured for five-years in St. 3 and St. 4 (Fig. 1), with a HOBO water level logger (model U20), placed 40 cm below the flat surface. The sensor recorded water level and temperature every 10 minutes. The HOBO sensor at St. 4 had been stolen before the March 2018 field trip, and thus, we lack data from October 2017-March 2018.

Permeability was measured both *in situ* on August 2018 at St. 4 and in the lab. Field measurements consisted on inserting a PVC cylindrical corer (19 cm long, inner diameter = 4 cm) into a water saturated surface covered with microbial mats with sand layers underneath until a 5.6 cm depth. Both in the field and lab, the core was filled to the top with seawater and the rate of infiltration of the water was measured in duplicate. This measurement was also repeated with a larger PVC cylindrical corer (1 m long, inner diameter = 11 cm), in two locations: where there was clear evidence of microbial mat presence and in an erosional pocket where there was little microbial mat colonization (Fig. 2b). For the larger PVC corer, we considered the time for the first 20 cm of the water column to permeate to perform our calculations, assuming a constant air-pressure. In the lab, unsaturated samples with and without the superficial microbial mat layer were tested. The size of lab samples was 11 x 7 cm with a thickness of 5 cm, and the same smaller field PVC core was inserted into the samples. Surficial microbial mats had a thickness of 7 mm.

2.3. Water and petrographic analysis

Water samples were routinely taken from St. 3, St. 4 and St. 3 Tidal Creek. Additionally, two TDs with at least 4 cm of water were chosen in St. 4 (St. 4 TD), with and without the presence of halite, and water samples from these TDs were also taken. Water sample salinity was determined gravimetrically according to Strickland and Parsons (1972). Main seawater ion concentrations (i.e. K^+, Ca^{2+}, Mg^{2+}, HCO_3^-, and SO_4^{2-}) were determined following standard methods from APHA (2005). A 10 % HCl solution was pipetted on site over the sediments, and carbonate presence was observed whenever effervescence occurred as a qualitative measure. Sediment cores were taken from the mat in cylindrical PVC tubes (7 cm long, inner diameter = 3 cm), which were cut longitudinally, and then, several layers were obtained at different depths to

157 prepare petrographic thin sections and for scanning electron microscopy with Energy-dispersive
158 X-ray spectroscopy (SEM with EDS; JEOL35 CF 8, Tokyo). Samples for SEM were fixed and
159 washed in a mixture of 2.5 % glutaraldehyde in Sorensen phosphate buffer. Afterwards, samples
160 were dehydrated in an acetone series (10 to 80 %), and last, they were dried by critical point and
161 coated with gold. Petrographic analyses were carried out by the use of analyzed under a NIKON
162 SMZ 1500 polarization microscope and a Nikon Eclipse 80*i* fluorescence optical microscope.
163 The nature of carbonate was determined by carbonate staining method described by Dickson
164 (1966), which consisted in dyeing the thin sections with alizarin red solution, hydrochloric acid
165 and $K_4Fe(CN)_6$. Halite crystals were determined in the field by their characteristic appearance at
166 a macroscopic scale. Gypsum precipitation was confirmed by XRD.

167 **3. Results**

168 *3.1. Permeability of microbial mats*

169 Two sites with different degree of sediment colonization were chosen to compare the
170 permeability over the Paso Seco flat. One site has a thick surficial microbial mat (~ 1 cm),
171 characterized by several old microbial mats beneath the surface, that covers the majority of the
172 flat; and the other was an erosional pocket, where the sediment is less colonized by microbes.
173 The average rate of permeation of infiltrated water in the field measured with the 1 m long PVC
174 tube was 37.63 cm^3 min^{-1} in the presence of microbial mats (Fig. 2a and c). In contrast, the water
175 permeated at a rate of 191.87 cm^3 min^{-1} over an erosional pocket (Fig. 2b and c). The same
176 experiment was performed in the presence of microbial mats with a smaller PVC tube (19 cm
177 long), and more than 66 % of the water volume remained in the PVC tube after 78 min had
178 passed (0.46 cm^3 min^{-1}). For the samples taken to the lab (also measured with the shorter PVC
179 tube), similar results of different magnitudes were found (Fig. 2c). The time water took to

permeate through the sample when the surficial microbial mat was removed (less than 3 minutes or an average of 79.1 cm^3 min^{-1}) was significantly shorter than both the measurements in the field and the untouched sample in the lab (more than 75 minutes or 1.92 cm^3 min^{-1}; Fig. 2c). Numerical differences between the different PVC tubes could be a result of the higher hydrostatic pressure in the larger tubes than in the smaller ones (capillarity phenomenon).

3.2. Fluctuations in water level and temperature

The characteristic fluctuation of the water level over the flats at Paso Seco and as groundwater can be seen in figure 3, where the floods and the exposed periods are recognized along three years. The water temperature in Austral winter was < 10°C and rose to above 20 ˚C in Austral summer. During winter, the groundwater level is close to the flat, and might be submerged by a sea-water lamina during several weeks after a flooding. In contrast, in summer (identified with rectangles in Fig. 3) the flat is sometimes flooded more often by seawater, but the flat is exposed to solar radiation during several days when the groundwater level fluctuates up to 0.50 m below the flat. In those occasions periods of evaporation (PE) might be possible.

Before the September 2017 field trip, the flat as a whole was occasionally covered with seawater (four times) during the two previous months before sampling, with water height less than 10 cm (Fig. 4a), and water temperature slowly raising from 10 to 15 °C in the days leading to the sampling date. Water last flooded the flat ten days before sampling, and subsequently the water level dropped, maintaining most of the flat exposed during eight days (PE, Fig. 4a) and the remaining seawater was only preserved in several TDs. During September 2017, weather conditions show rising high daily temperatures with the maximum temperature ranging between 20-25 ˚C five days before the sampling (Fig. 4b) and moderate winds between 20 to 36 km h^{-1}, predominately coming from the NW (Fig. 4c). These winds in the region are very dry,

reinforcing the evaporation process. Thus, these conditions were conducive to a period of evaporation (PE) on the exposed flat.

3.4. Evaporite presence

During the September 2017 field trip, TDs at St. 4 exposed rings of precipitated salts that marked where the seawater had been before evaporating (Fig. 5a). Carbonate was detected in the flat by HCl test (confirmed as calcite by thin sections), and sheets of gypsum (confirmed by XRD) and halite crystals were found both in TDs and on the microbial mats after complete evaporation (Fig. 5b-d).

SEM with EDS and petrographic analyses of thin sections of the microbial mats were carried out displaying similar results. EDS analyses demonstrated that repeated thin layers of cation Ca^{2+} are present in a sedimentary corer (Fig. 6). Likewise, petrographic thin section exhibited 100-200 µm-thick layers of dense micritic calcite within the microbial mats (Fig. 7).

3.5. Water salinity and composition

The values for the three sites (St. 3, St. 3 Tidal Creek, and St. 4) varied throughout the study period (Fig. 8a); however, St. 3 always had the highest salinity values, followed by St. 4, and lastly, St. 3Tidal Creek, which still presented salinity values much higher than the expected seawater value. The lowest value, 49.4 g L^{-1}, occurred in St. 4 in May and the highest salinity, 115 g L^{-1}, was found in St. 3 in September (Austral spring; Fig. 8a). In June 2018, the salinity of the water flooding the flat was 62.8 and 52.4 g L^{-1}, at St. 3 and St. 4, respectively. At two of the sampling dates (September 2017 and March 2018), water samples were also taken from TDs – with and without halite crystals –having salinities higher than 200 g L^{-1} (Fig. 8b).

Water from St. 3, St. 3 Tidal Creek, St. 4 and two TDs (with and without halite precipitation) was collected in September 2017 and analyzed to obtain its ion concentration

(Table 1). The comparison between TDs shows that as salinity increased at the different sites measured with regards to seawater salinity, Ca^{2+} concentrations increased reaching a maximum value in a clear TD (with no halite precipitated) (Table 1). For salinities higher than 250 g L^{-1}, where precipitated halite was found, Ca^{2+} concentrations dropped to values of less than 30 mEq L^{-1} (Fig. 8c). Conversely, both Mg^{2+} and SO_4^{2-} concentrations rose as salinity increased and always remained higher than the one for Ca^{2+} (Table 1). Equally, the concentration of HCO_3^- was always lower than the one for Ca^{2+}. The ratio of Mg^{2+}/Ca^{2+} also behaved in a similar fashion, dramatically increasing whenever precipitated halite was found.

4. Discussion

Paso Seco's saline-like behavior during summer is found outside the subtropical high-pressure belts where most marginal marine evaporitic environments are usually found (Babel and Schreiber, 2014). Similar to the Mediterranean sabkhas (Warren, 2016a), Paso Seco is a periodically flooded coastal flat, with little vegetation (Cuadrado et al., 2015). Salinity of the pore water in St. 3 when the flat is subaerially exposed is within the same range as the pore water of the saline zone (between 95 and 160 g L^{-1}) in sabkhas located between Sulaymaniya lagoon and Sharm Obhur (Bahafzullah et al., 1993), and the Al-Kharrar sabkha (Aref and Taj, 2017), among others. St. 3 receives water both from the sea and the St. 3 tidal creek, which lead to salt precipitation due to water evaporation, and later, as the next flood enters the flat, these salts are then diluted, increasing the saltwater values. The coastal flat, also in a similar fashion to sabkhas, is covered with a thick microbial mat layer (up to 1 cm), which shows little grazing as salinity in most stations and on the flat is higher than what gastropods and other predators can stand (Cornée et al., 1992). The main difference between the location in the present study and low-latitudes sabkhas characterized by arid climate mainly revolves around the higher amount of

249 rainfall that the study site receives yearly. This condition would affect the redissolution of the
250 evaporites, explaining the small amounts of intra-sedimentary gypsum and halite found on site.
251 Weather conditions at the Paso Seco site are also favorable for water evaporation, as the
252 coastal flat surface is exposed to evaporation because of the rise in air temperature (>20 ˚C),
253 reinforced by moderate wind speed (20-36 km h^{-1}; Fig 6c) during PE. Water evaporation is
254 evidenced by, first, the evaporation rings in the coastal flat (Fig. 5a); and second, by the visual
255 presence of both gypsum and halite (Fig. 5b, c and d), as well as $CaCO_3$ (Fig. 6), as the Usiglio
256 sequence predicts (Usiglio, 1849; Warren, 2016c). $CaCO_3$ would crystalize when the solute
257 concentration reaches twice the concentration of seawater, followed by gypsum and later, by
258 halite precipitation (Usiglio, 1849), as was sustained by the chemical analysis (Table 1).
259 Hardie and Lowestein (2003) also followed the ion concentrations in seawater as water
260 evaporates and determined two important divides for the formation of brines of different
261 composition: the $CaCO_3$ and the gypsum divides. As seawater evaporates, Ca^{2+} concentrations
262 increase up to the point where, if the concentration of Ca^{2+} is higher than the concentration
263 HCO_3^-, all HCO_3^- precipitates as $CaCO_3$ and the remaining Ca^{2+} will start precipitating as
264 gypsum (Babel and Schreiber, 2014; Hardie and Lowenstein, 2003), as can be seen in the Paso
265 Seco site (Fig. 9 and Table 1). Gypsum precipitation begins at salinities of 150 g L^{-1} and
266 continues until salinity reaches between 290 and 320 g L^{-1} (Logan, 1987; Usiglio, 1849),
267 salinities that are reached at the different TDs. This precipitation is also favored by the presence
268 of microbial mats in the surface (Oren, 2010). After gypsum precipitation, when the
269 concentration of SO_4^{2-} is high as can be found in Paso Seco (Table 1), the concentration of Ca^{2+}
270 in water falls abruptly (Babel and Schreiber, 2014; Hardie and Lowenstein, 2003) because it
271 precipitates as $CaSO_4$ over the inundated flat (Figs. 5 and 9). At the same time, the ratio of

272 Mg^{2+}/Ca^{2+} in the evaporating water rapidly increases after the precipitation of gypsum, which we
273 have also seen both in the most evaporated samples (TDs; Table 1 and Fig. 8). That fact was
274 corroborated in sedimentary cores where thin layers of calcite were recognized by EDS and
275 petrographic analysis (Figs. 6 and 7).

276 As seen with the presence of evaporites at the site, Paso Seco behaves as a saline-like basin
277 that has evolved to total dryness during summer months (Fig. 10) (Bąbel, 2007; Babel and
278 Schreiber, 2014). From September until April (Austral spring, summer and beginning of fall),
279 seawater enters the coastal flat as it overcomes the sand barrier during storms. The main outflow
280 of seawater is through ebbing; however, the presence of microbial mats covering all the surface
281 of this saline-like flat is able to retain enough seawater for it to be evaporated during periods of
282 warm temperatures and moderate winds that occur when the flat is exposed. This effect is
283 mediated through the semi-pervious property that the microbial mats convey to the surface.
284 Additionally, the alkaline pH microbial mats develop help maintain seawater pH and thus, favors
285 $CaCO_3$ precipitation (Dupraz et al., 2009). However, the periodic water input from each storm
286 dissolves the precipitated gypsum and halite in the TDs, of which only few precipitates remain
287 (Fig. 6), and most probably modifies the thickness of the precipitated $CaCO_3$ layer (Babel and
288 Schreiber, 2014; Sanford and Wood, 1991).

289 Microbial mats have poor permeability as can be seen already at the Paso Seco site by gas
290 domes formed as typical microbial sedimentary structures. These structures are generated from
291 intra-sedimentary gas pressure producing a flexible deformation microbial mat preventing the
292 escape of gases (Cuadrado et al., 2015; Gerdes, 2007). Also, with a simple field test, we
293 determined that with microbial mats covering the surface, the coastal flat behaves as semi-
294 pervious surface, similar to how unconsolidated very fine sands, silts, and loams behave (Bear,

2013). The copious sheath material secreted by *Microcoleus chthonoplastes*, a species found in Paso Seco's microbial mats (Cuadrado and Pan, 2018), provides cohesiveness to the sediment and helps retain water (Stal, 2000; Stolz, 2000) where microbial mats are present. In contrast, the erosional pockets, structures characterized by bottom ripples formed by tidal currents due to less colonized sand (Noffke, 1999), water permeability is higher, determining that permeability is related to sediment colonization. Moreover, we also obtained a similar result in the lab as in the field, and when the microbial mat was removed, the remaining layer permitted water permeation at a significantly higher rate, which leads to conclude that without the microbial mat, the behavior of the coastal flat would resemble a pervious surface.

5. Conclusion

This paper documents the biological effect that microbial mats have on the hydrology of a coastal area. In spite that Paso Seco is located at medium-latitudes, it behaves similar to a low-latitude coastal sabkha during the summer months, with a semi-arid climate favorable for evaporite formation. Seawater enters the coastal flat during a storm, and after most of the water has ebbed, what remains is retained on the flat thanks to the increased impermeability that the microbial mats confer to the surface, providing a significant barrier for water infiltration. Without the biological action of these microbial mats, water would infiltrate through the sandy sediment instead of remaining on the surface for longer periods of time. This water retention results in evaporite formation as water evaporates when temperatures rise and drying winds prevail. Thin calcite layers in the microbial mats record the evolution of the flat to total dryness.

Studies made in the last thirty years are demonstrating that microbial mats are very common in all type of environments (being found also in fossil records), but seldom studied in relation to how their presence affects the hydrology. This paper confirms that the presence of

318 microbial mats provides a significant barrier for water infiltration deeply affecting results dealing
319 with water percolation and evaporation processes.
320
321 **6. Acknowledgements**
322 We would like to thank Dr. Eduardo A. Gomez, Angie Speake and Luis Ariel Raniolo for
323 their help during the fieldwork.
324 Funding: This research was supported by CONICET (grant PIP 2013 N°4061), SECYT-
325 UNS (grant PGI 24/H138), and the Spanish José Castillejo program (grants CAS16/00124 and
326 CAS17/00270).
327 **7. References**
328 Aliaga, V.S., Ferrelli, F., Piccolo, M.C., 2017. Regionalization of climate over the Argentine
329 Pampas. Int. J. Climatol. 37, 1237–1247.
330 Alvarez, H.M., Silva, R.A., Cesari, A.C., Zamit, A.L., Peressutti, S.R., Reichelt, R., Keller, U.,
331 Malkus, U., Rasch, C., Maskow, T., 2004. Physiological and morphological responses of
332 the soil bacterium Rhodococcus opacus strain PD630 to water stress. FEMS Microbiol.
333 Ecol. 50, 75–86.
334 APHA, 2005. Standard methods for the examination of water and waste water, 21st ed.
335 American Public Health Association, Washington, DC.
336 Aref, M.A., Taj, R.J., 2017. Hydrochemical characteristics of sabkha brines, evaporite
337 crystallization and microbial activity in Al-Kharrar sabkha and their implication on future
338 infrastructures in Rabigh area, Red Sea coastal plain of Saudi Arabia. Environ. Earth Sci.
339 76, 360.

340 Aref, M.A., Taj, R.J., 2018. Recent evaporite deposition associated with microbial mats, Al-
341 Kharrar supratidal–intertidal sabkha, Rabigh area, Red Sea coastal plain of Saudi Arabia.
342 Facies 64.
343 Bąbel, M., 2007. Badenian Gypsum Facies as a Model Salina-Type Basin Deposit, in: Schreiber,
344 B.C., Lugli, S., Babel, M. (Eds.), Evaporites Through Space and Time. Geological
345 Society of London, London, Special Publication, pp. 107–142.
346 Babel, M., Schreiber, B.C., 2014. Geochemistry of evaporites and evolution of seawater. Treatise
347 Geochem. 483–560.
348 Bahafzullah, A., Fayed, L.A., Kazi, A., Al-Saify, M., 1993. Classification and distribution of the
349 red sea coastal sabkhas near Jeddah-Saudi Arabia. Carbonates Evaporites 8, 23.
350 Bear, J., 2013. Dynamics of fluids in porous media. Courier Corporation.
351 Butler, G.P., Harris, P.M., Kendall, C.S.C., 1987. Recent evaporites from the Abu Dhabi coastal
352 flats.
353 Cornée, A., Dickman, M., Busson, G., 1992. Laminated cyanobacterial mats in sediments of
354 solar salt works: some sedimentological implications. Sedimentology 39, 599–612.
355 Cuadrado, D.G., Bournod, C.N., Pan, J., Carmona, N.B., 2013. Microbially-induced sedimentary
356 structures (MISS) as record of storm action in supratidal modern estuarine setting.
357 Sediment. Geol. 296, 1–8.
358 Cuadrado, D.G., Pan, J., 2018. Field Observations On the Evolution of Reticulate Patterns in
359 Microbial Mats in a Modern Siliciclastic Coastal Environment. J. Sediment. Res. 88, 24–
360 37.
361 Cuadrado, D.G., Pan, J., Gómez, E.A., Maisano, L., 2015. Deformed microbial mat structures in
362 a semiarid temperate coastal setting. Sediment. Geol. 325, 106–118.

363 Dean, W.E., 2013. Marine Evaporites, in: Harff, J., Meschede, M., Petersen, S., Thiede, J. (Eds.),
364 Encyclopedia of Marine Geosciences. Springer Netherlands, Dordrecht, pp. 1–10.
365 Decho, A.W., 2011. Extracellular Polymeric Substances (EPS), in: Reitner, J., Thiel, V. (Eds.),
366 Encyclopedia of Geobiology, Encyclopedia of Earth Sciences Series. Springer
367 Netherlands, pp. 359–362.
368 Dickson, J.A.D., 1966. Carbonate identification and genesis as revealed by staining. J. Sediment.
369 Res. 36, 491–505.
370 Dupraz, C., Reid, R.P., Braissant, O., Decho, A.W., Norman, R.S., Visscher, P.T., 2009.
371 Processes of carbonate precipitation in modern microbial mats. Earth-Sci. Rev. 96, 141–
372 162.
373 Ferrelli, F., Bohn, V.Y., Piccolo, M.C., 2012. Variabilidad de la precipitación y ocurrencia de
374 eventos secos en el sur de la provincia de Buenos Aires (Argentina). IX Jornadas
375 Nacionales de. Geografía Fisica 15–28.
376 Flemming, H. C., Wingender, J., 2001. Relevance of microbial extracellular polymeric
377 substances (EPSs) - Part I: Structural and ecological aspects. Water Sci. Technol. 43, 1–8.
378 Gerdes, G., 2007. Structures left by modern microbial mats in their host sediments, in: Atlas of
379 Microbial Mat Features Preserved within the Siliciclastic Rock Record. Elsevier
380 Amsterdam, pp. 5–38.
381 Hardie, L.A., Lowenstein, T.K., 2003. Evaporites, in: Sedimentology. Springer Netherlands,
382 Dordrecht, pp. 416–426.
383 Kinsman, D.J., 1976. Evaporites; relative humidity control of primary mineral facies. J.
384 Sediment. Res. 46, 273–279.

385 Krumbein, W.C., Garrels, R.M., 1952. Origin and classification of chemical sediments in terms
386 of pH and oxidation-reduction potentials. J. Geol. 60, 1–33.
387 Logan, B.W., 1987. The MacLeod evaporite basin, Western Australia: Holocene environments,
388 sediments and geological evolution. American Association of Petroleum Geoglogists.
389 Long, D.T., Lyons, W.B., Hines, M.E., 2009. Influence of hydrogeology, microbiology and
390 landscape history on the geochemistry of acid hypersaline waters, N.W. Victoria. Appl.
391 Geochem., Natural Low-pH Environments Unaffected by Human Activity 24, 285–296.
392 Noffke, N., 1999. Erosional remnants and pockets evolving from biotic–physical interactions in a
393 Recent lower supratidal environment. Sediment. Geol. 123, 175–181.
394 Or, D., Smets, B.F., Wraith, J.M., Dechesne, A., Friedman, S.P., 2007. Physical constraints
395 affecting bacterial habitats and activity in unsaturated porous media–a review. Adv.
396 Water Resour. 30, 1505–1527.
397 Oren, A., 2010. Thoughts on the "missing link" between saltworks biology and solar salt quality.
398 Glob. NEST J 12, 417–425.
399 Orti, F., 2010. Evaporitas: formaciones marinas y continentales. Algunos ejemplos. Sedimentol.
400 Proceso Fısico Cuenca Sedimentaria Madr. Cons. Super. Investig. Cientıficas 771–838.
401 Perillo, G.M.E., 2018. Geomorphology of Tidal Courses and Depressions, in: Perillo, G.M.E.,
402 Wolanski, E., Hopkinson, C. (Eds.), Coastal Wetlands: An Integrated Ecosystem
403 Approach. Elsevier, pp. 221–261.
404 Sanford, W.E., Wood, W.W., 1991. Brine evolution and mineral deposition in hydrologically
405 open evaporite basins. Am. J. Sci. 291, 687–710.
406 Schnider-Keel, U., Lejbølle, K.B., Baehler, E., Haas, D., Keel, C., 2001. The Sigma Factor AlgU
407 (AlgT) Controls Exopolysaccharide Production and Tolerance towards Desiccation and

Osmotic Stress in the Biocontrol Agent Pseudomonas fluorescensCHA0. Appl. Environ. Microbiol. 67, 5683–5693.

Servicio Meteorologico Nacional. [WWW Document], n.d. URL https://www.smn.gob.ar/clima/atlasclimatico (accessed 4.16.19).

Shearman, D.J., 1978. Evaporites of coastal sabkhas. Mar. Evaporites 4, 6–42.

Stal, L.J., 2000. Cyanobacterial Mats and Stromatolites, in: Whitton, B.A., Potts, M. (Eds.), The Ecology of Cyanobacteria: Their Diversity in Time and Space. Springer Netherlands, Dordrecht, pp. 61–120.

Stolz, J.F., 2000. Structure of microbial mats and biofilms, in: Microbial Sediments. Springer, pp. 1–8.

Strickland, J.D., Parsons, T.R., 1972. A practical handbook of seawater analysis.

Strohmenger, C.J., Shebl, H., Al-Mansoori, A., Al-Mehsin, K., Al-Jeelani, O., Al-Hosani, I., Al-Shamry, A., Al-Baker, S., 2010. Facies stacking patterns in a modern arid environment: a case study of the Abu Dhabi sabkha in the vicinity of Al-Qanatir Island, United Arab Emirates. Quat. Carbonate Evaporite Sediment. Facies Their Anc. Analog. Tribute Douglas James Shear. 149–182.

Twenhofel, W.H., 1950. Principles of sedimentation, 2nd ed. McGraw-Hill, New York.

Usiglio, M.J., 1849. Etudes sur la composition de l'eau de la Mediterranee et sur l'exploitation des sels qu'elle contient. Ann. Chim Phys Ser 3 27, 172–191.

Warren, J.K., 2016a. Sabkhas, Saline Mudflats and Pans, in: Warren, J.K. (Ed.), Evaporites: A Geological Compendium. Springer International Publishing, Cham, pp. 207–301. https://doi.org/10.1007/978-3-319-13512-0_3

Warren, J.K., 2016b. Subaqueous Salts: Salinas and Perennial Lakes, in: Warren, J.K. (Ed.), Evaporites: A Geological Compendium. Springer International Publishing, Cham, pp. 303–380. https://doi.org/10.1007/978-3-319-13512-0_4

Warren, J.K., 2016c. Depositional Chemistry and Hydrology, in: Warren, J.K. (Ed.), Evaporites: A Geological Compendium. Springer International Publishing, Cham, pp. 85–205. https://doi.org/10.1007/978-3-319-13512-0_2

***Declaration of Interest Statement**

Declaration of interests

☒ The authors declare that they have no known competing financial interests or personal relationships that could have appeared to influence the work reported in this paper.

☐The authors declare the following financial interests/personal relationships which may be considered as potential competing interests:

Graphical Abstract (for review)

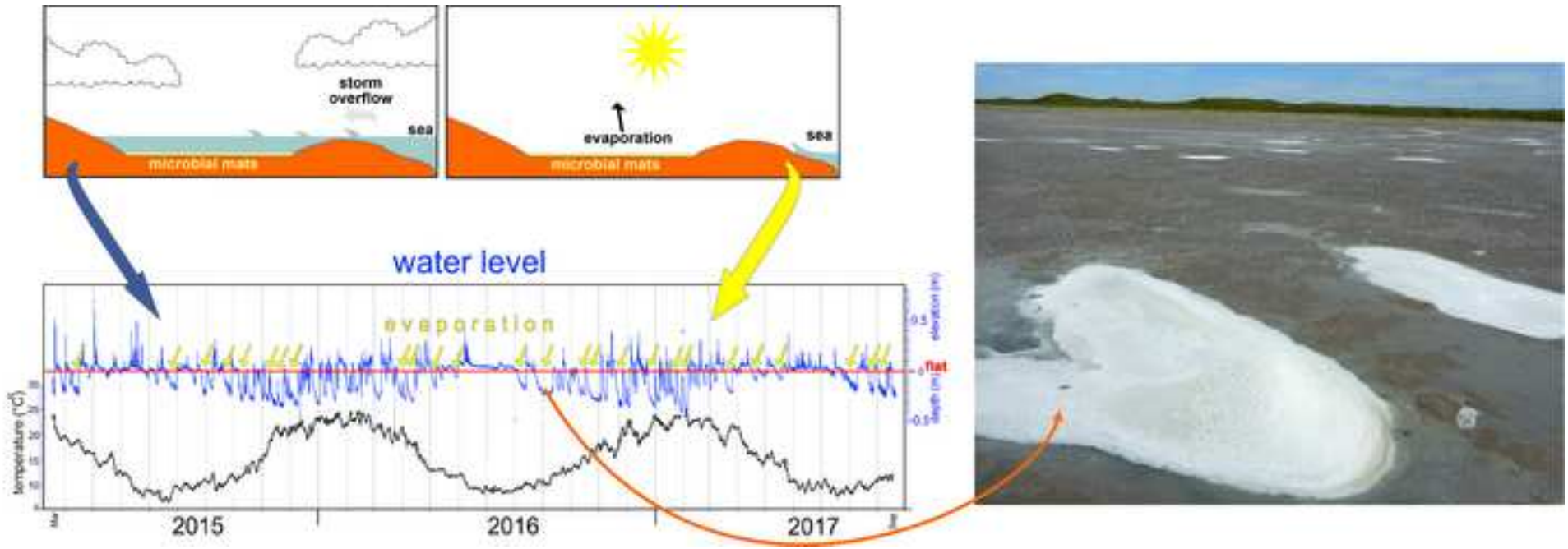

Table 1.

Ion concentrations and Mg^{2+}/Ca^{2+} ratio (September 2017)

Station	Salinity ($g\ L^{-1}$)	SO_4^{2-} ($mEq\ L^{-1}$)	Mg^{2+} ($mEq\ L^{-1}$)	Ca^{2+} ($mEq\ L^{-1}$)	HCO_3^- ($mEq\ L^{-1}$)	Mg^{2+}/Ca^{2+}
Sea	34.29	55.2	103.9	20.0	2.3	3.2
St. 3 Tidal Creek	67.95	77.4	143.5	31.5	3.0	2.8
St. 3	115.37	109.81	268.5	42.8	3.2	3.8
St. 4	91.66	113.0	244.5	38.0	5.02	3.9
St. 4 TD	202.51	310.4	604.0	53.5	1.94	6.9
St. 4 TD Halite	279.41	477.3	915.0	22.5	5.81	24.7

Figure Captions

Figure 1. Study site. Location and sampling stations: St. 3 Tidal creek (40°38'42.20"S; 62°13'4.81"W), St. 3 (40°38'39.32"S; 62°13'1.72"W), and St. 4 (40°38'3.32"S; 62°12'24.85"W).

Figure 2. Tidal depressions and erosional pocket surface. (a) Overview of the coastal flat with depressions where water remains (red arrow shows the predominant NW wind direction). (b) Erosional pocket with ripples overlain by halite. (c) Permeated seawater volume through microbial mats in the field and in the lab, contrasted to permeated volume after mat was removed (both in field and in the lab, and with different PVC tube sizes).

Figure 3. Flooding frequency and periods of exposition. Flood and evaporation frequency at sampling station St. 4 starting March 2015 and ending on September 2017. The blue line shows water level, with flooding events showing over the red line (flat surface), while all events below the line show the level of the water table (below the surface). The yellow squares show the austral summer and spring, periods where groundwater levels are lower and the plain is exposed for longer periods of time. The black line shows water temperature (˚C).

Figure 4. Weather and hydrodynamic data leading to the September 2017 sampling trip. (a) Flood and evaporation frequency at sampling station St. 4 starting August 2017 and ending on the sampling date. The green line shows water level, with flooding events showing over the red line (flat surface), while all events below the line show the level of the water table (below the surface) and also, periods of evaporation (PE). The blue line shows water temperature (˚C). (b)

Daily air temperature and wind speed during the previous twenty days before sampling in September 2017. The light blue and orange lines correspond to PE and match the two lines of the same color show in (a). Black circles highlight the maximum temperature for each day.

Figure 5. Evaporites in field site. Black arrows show evaporation rings during eight days after the last flooding of the coastal flat (a). Gypsum sheets (b). Halite crystals were observed both in water-filled and in completely evaporated TDs (c and d, respectively).

Figure 6. Energy dispersive X-ray spectrometry (EDS) maps of the same fragment. Repeated Ca^{2+} layers in depth, some co-locating with S, probably in association with gypsum. Low presence of Na^{+} and Cl^{-} co-location (probably association with halite).

Figure 7. Thin section of the Paso Seco flat. Microbial mats that colonize the flats are organized in successive laminae composed of sand, silt, clay and organic matter. Micritic carbonate laminae (arrows) are found interbedded within the microbial mats. (a) Cross polarized light. (b) Plane polarized light.

Figure 8. Evaporite precipitation after sea water evaporation. (a) Salinity concentration (g L^{-1}) in the different stations. (b) Comparison between September 2017 and March 2018 on salinity in the different stations and tidal depressions. (c) Calcium concentrations (mEq L^{-1}) in the different stations for September 2017 and March 2018 sampling dates.

Figure 9. Evaporite precipitation pathway. Evaporation rings after sea water evaporation (1). After $CaCO_3$ precipitation (black arrows and dashed white lines), we observed the presence of gypsum because of the higher Ca^{2+} concentration over HCO^{3-} found in the water (2). Last, halite crystals were observed because of the higher SO_4^{2-} concentration over Ca^{2+} in the TDs that had halite (3). Modified from Hardie and Lowenstein, 2003.

Figure 10. Salina-like behavior in Paso Seco, Argentina. During the warmer months of the year (September through April), the flat suffers periodic flooding due to storm surge overflow with the consequent accumulation of water in TD due to the presence of poorly permeable microbial mats that cover the otherwise very permeable sands. This water accumulation is followed by several days of warm weather and moderate winds, allowing for water evaporation and the subsequent evaporites found precipitated on the flat (photo).

Figure 1

Click here to download high resolution image

Figure 2

Click here to download high resolution image

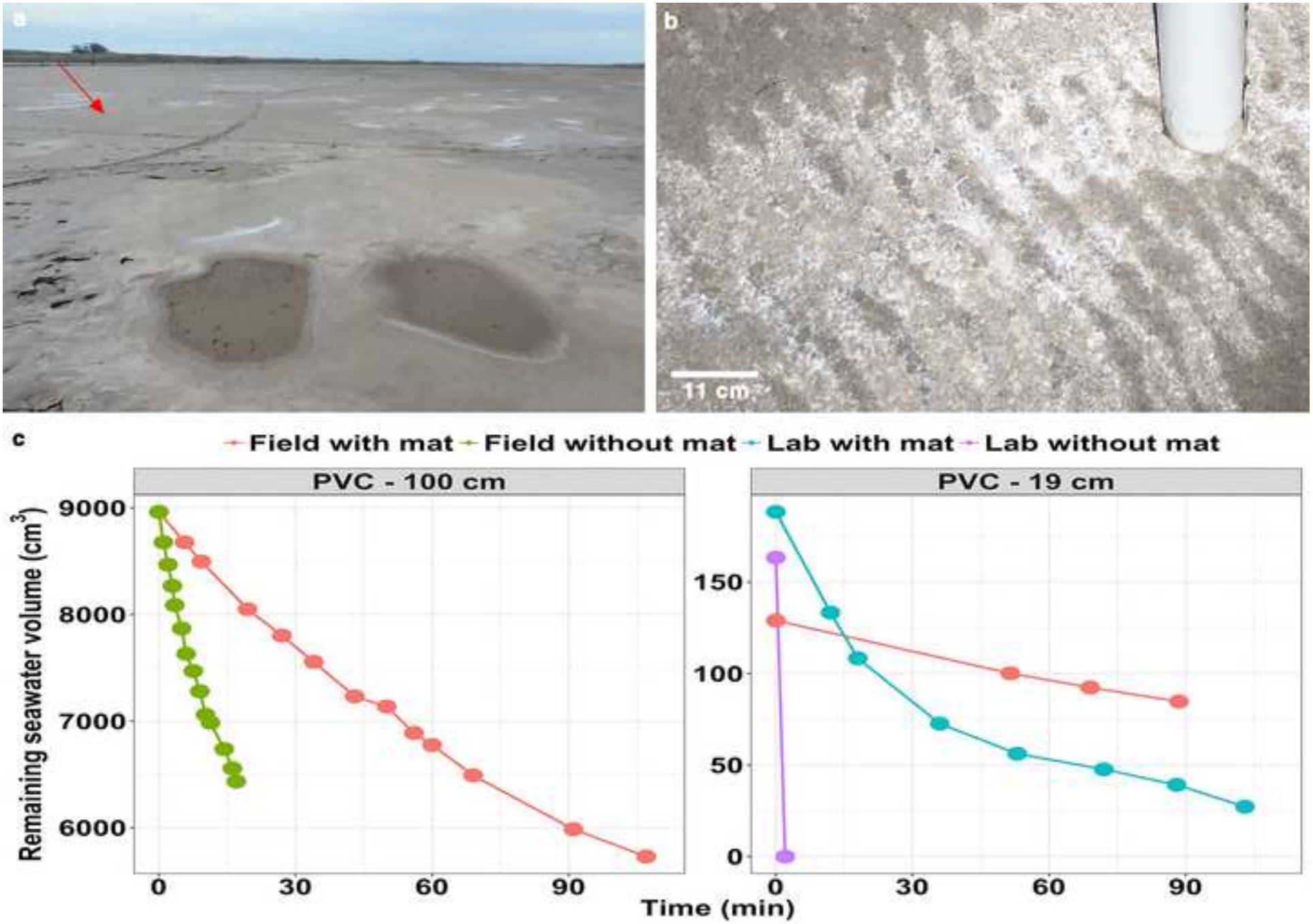

Figure 3

Click here to download high resolution image

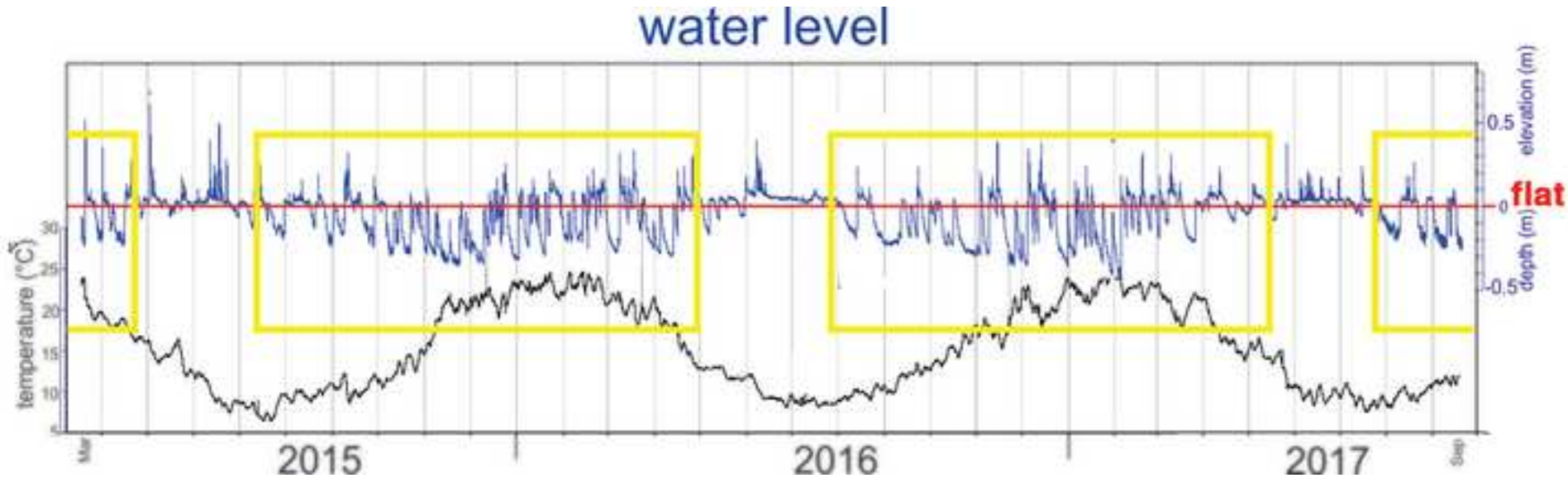

Figure 4

Click here to download high resolution image

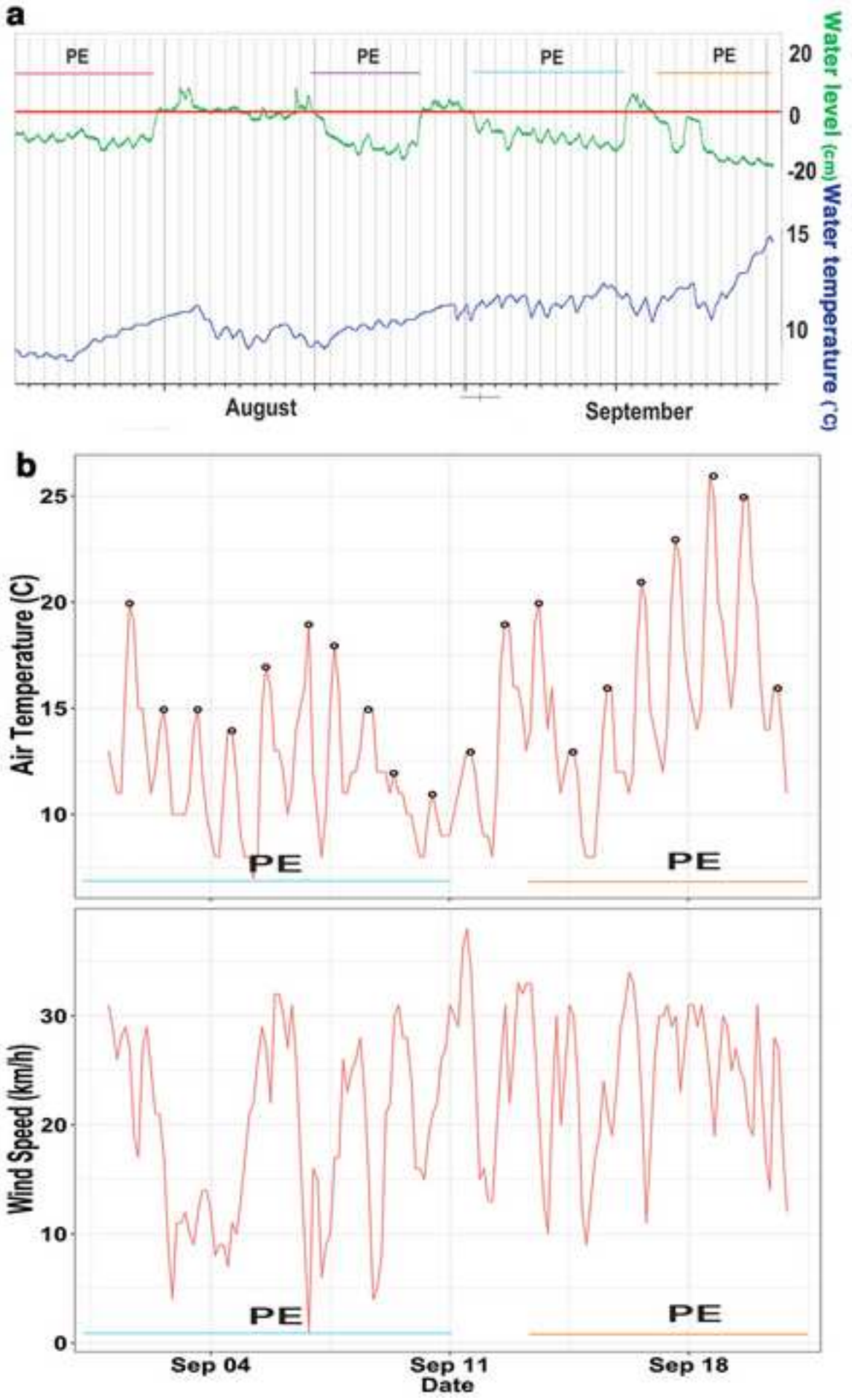

Figure 5

Click here to download high resolution image

Figure 6

Click here to download high resolution image

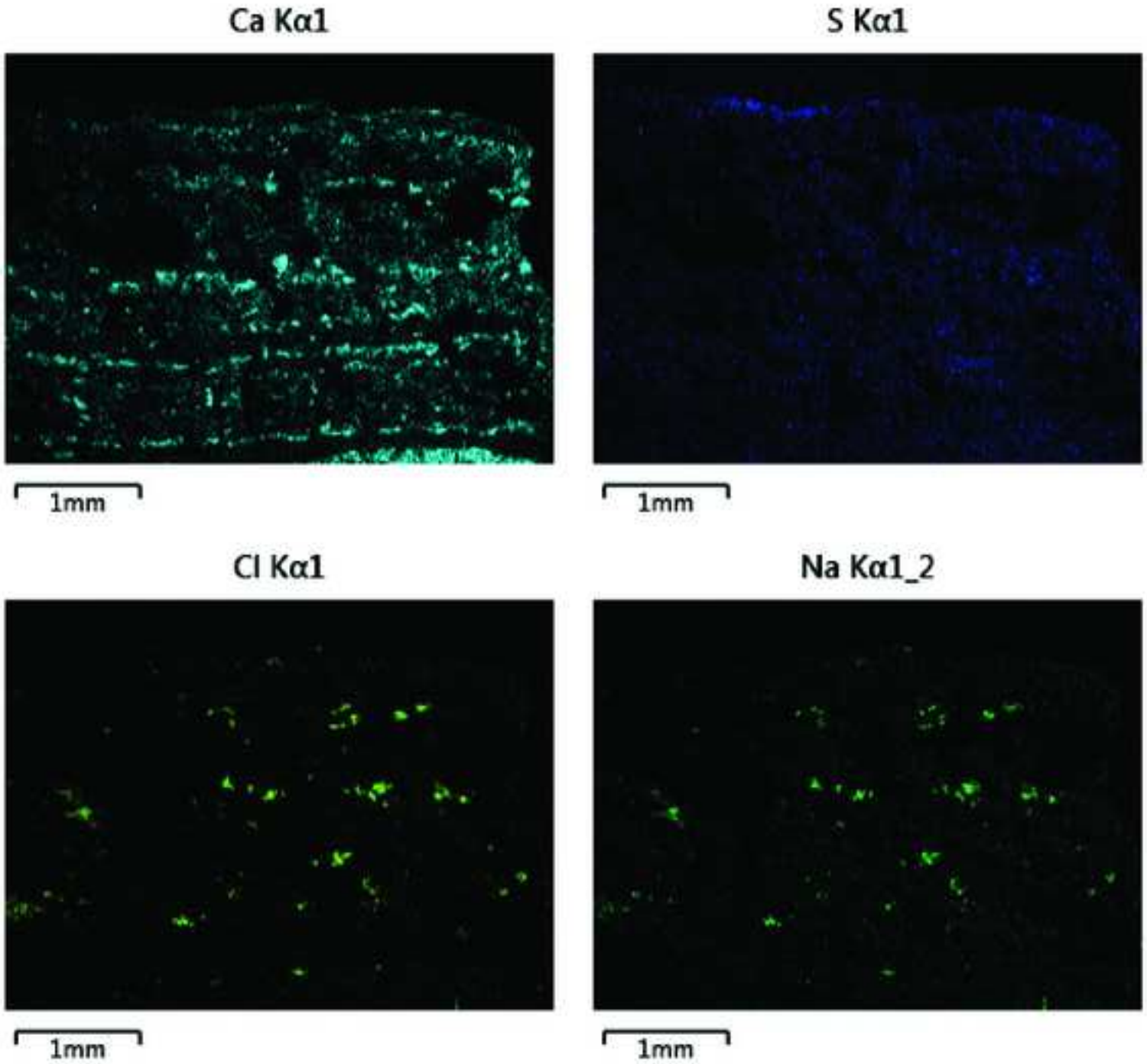

Figure 7

Click here to download high resolution image

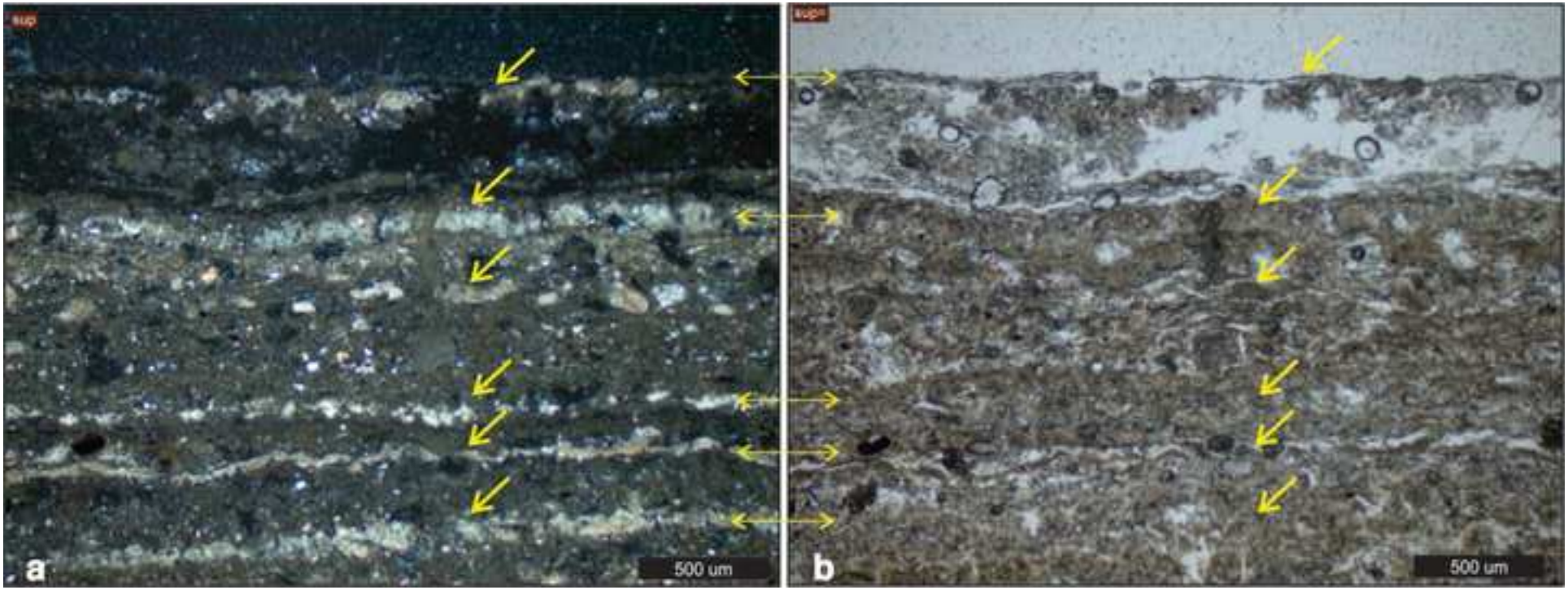

Figure 8

Click here to download high resolution image

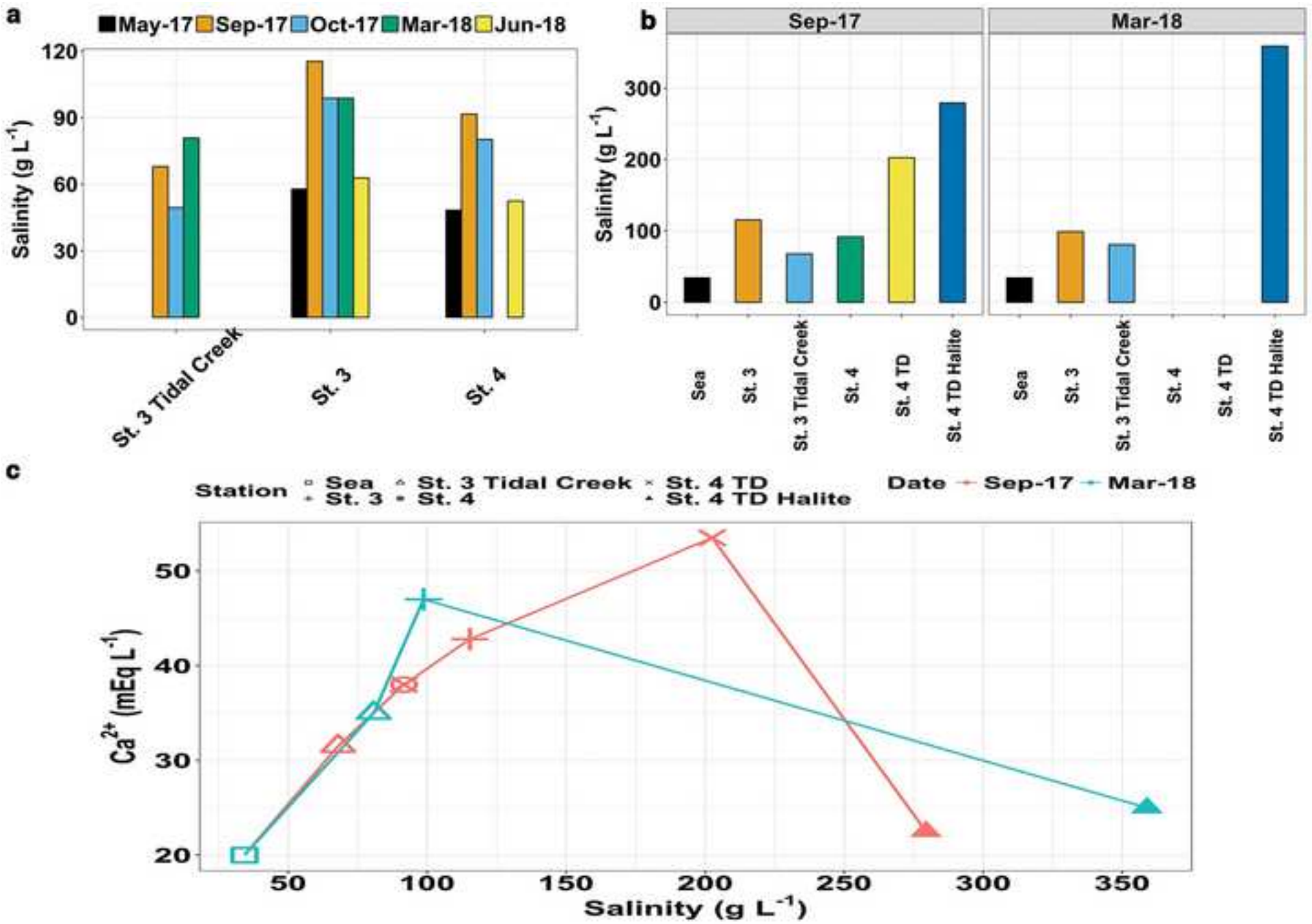

Figure 9

Click here to download high resolution image

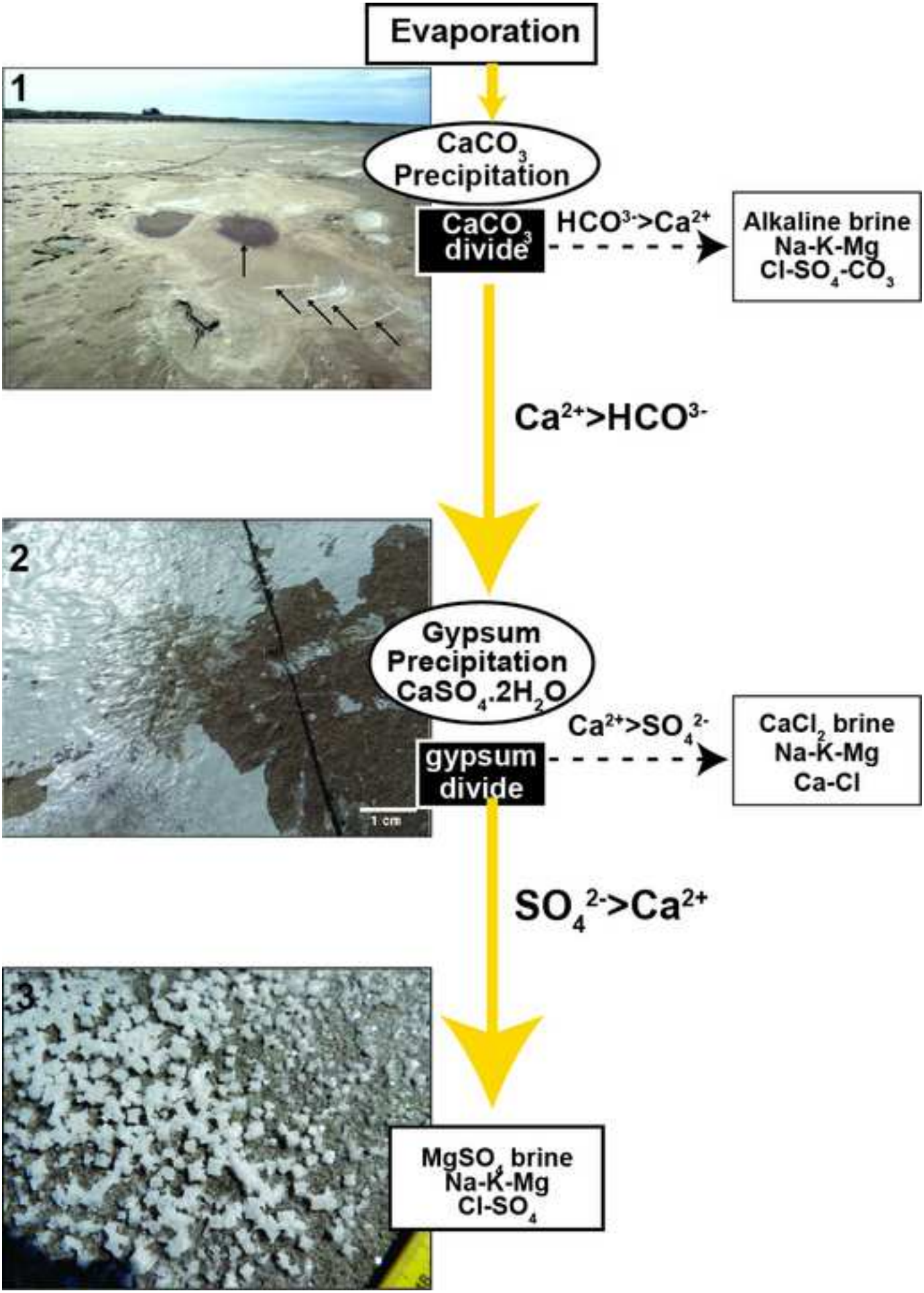

Figure 10

Click here to download high resolution image

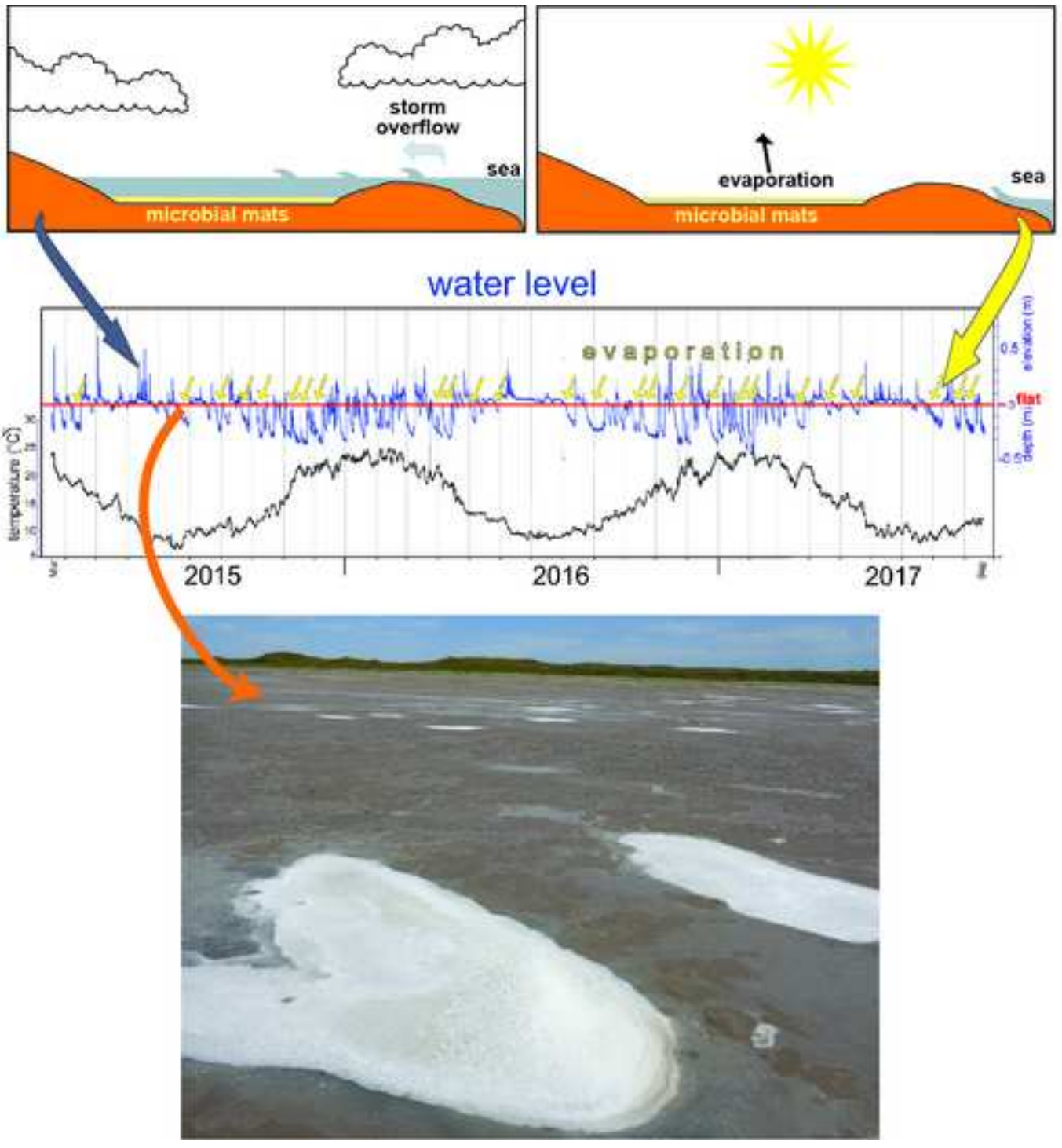

CRediT author statement

Vanesa L. Perillo: Conceptualization; Data curation; Investigation; Methodology; Resources; Visualization; Writing - original draft; Writing - review & editing. **Lucía Maisano**: Conceptualization; Data curation; Investigation; Visualization; Resources; Writing - review & editing. **Ana M. Martinez:** Investigation; Resources; Writing - review & editing. **I. Emma Quijada:** Conceptualization; Investigation; Visualization; Writing - review & editing. **Diana G. Cuadrado:** Conceptualization; Funding acquisition; Investigation; Methodology; Project administration; Resources; Supervision; Visualization; Writing - review & editing.